RANDOM SAMPLING STRATEGIES IN MULTISTATIC SAR

Jonathan D. Coker and Ahmed H. Tewfik

University of Minnesota
Department of Electrical and Computer Engineering

ABSTRACT

We introduce and investigate the concept of random sampling to the problem of image reconstruction in a multistatic SAR system. We first develop an appropriate figure of merit for the invertibility of the measurement data. We then show numerical simulations of a particular random measurement process under various parameters and compare the performance of this random sampling to that of the sampling given by a deterministic elliptical transform. We expose new connections between SAR processing and random matrix theory, and develop a fundamental result relating image quality to SAR system parameters for this mode.

Index Terms— Synthetic aperture radar, Radon transforms, tomography

1. INTRODUCTION

In [1], we extended the previous monostatic work of Redding [2], Milman [3], Norton[4], and others, by generalizing the SAR geometries to treat the case of a multistatic system of SAR transmitters and receivers in arbitrary three dimensional orbits over a flat, two-dimensional reflectivity plane. We observed that an impulsive radar burst between a transmit/receive pair measures a sequence of line integrals of the reflectivity over a set of ellipses. We defined an elliptical Radon transform, $\mathcal{R}_e f$, of a two dimensional reflectivity function f. This transform describes the measurements taken by a bistatic pair moving together with a constant velocity vector. We used a variation of the *approximate inverse* technique to invert $\mathcal{R}_e$.

In recent work, Yazici, Yarman, and Cheney [5] have developed a similar tomographic formulation of the bistatic SAR problem. In contrast to that work, we have chosen to apply the tools of linear algebra by casting the inversion in terms of a sparse matrix equation

$$\mathbf{A}\hat{\mathbf{f}} = \mathbf{r}_e \tag{1}$$

where $\mathbf{A}$ is a large sparse $m \times n$ matrix representing n image pixels and m measurements, $\hat{\mathbf{f}}$ is an unknown vector representing a reflectivity estimate of each pixel in the image, and $\mathbf{r}_e$ is the measurement vector. Each element of $\mathbf{r}_e$ is a measurement of the line integral of the reflectivity function around an ellipse.

In this present work, we examine the consequences of *random sampling* on the performance of the image reconstruction process. Our main contributions are the derivation of a specific random sampling approach for multistatic SAR, and the relationship between image quality and SAR system parameters. We consider the inversion problem in which a large number of SAR vehicles are moving in uncoordinated fashion over the field of interest. To these ends, we first develop an appropriate figure of merit for the invertibility of the measurement data. We then show numerical simulations of a particular random measurement process under various parameters and compare the performance of this random sampling to that of the sampling given by the deterministic elliptical transform $\mathcal{R}_e f$. We expose new connections between SAR processing and random matrix theory.

Our proposed approach can be compared and contrasted to the related area of compressed sensing (CS), c.f., [6, 7]. In terms of equation 1, CS recovers an image $\hat{\mathbf{f}}$ from the random projections $\mathbf{r}_e$, by assuming that $\hat{\mathbf{f}}$ is sparse in some basis. In this case, m can be less than n. In common with CS, our approach employs in-some-sense-random projections defined by the matrix $\mathbf{A}$. However, we make no assumption about the compressibility of the image $\hat{\mathbf{f}}$; generally, $m > n$ in this work. We emphasize the consequences of $\mathbf{A}$'s sparsity, rather than that of the image.

2. INVERSION FIGURE OF MERIT

Inversion algorithms suffer from impediments arising from a variety of causes. In this work, we shall focus on those error mechanisms which depend solely on the sampling strategy and not on the details of the image to be reconstructed.

It can be shown that in the presence of Gaussian measurement noise, a maximum likelihood image estimate $\hat{\mathbf{f}}_{ML}$ is found by the standard least-squares solution:

$$\begin{aligned}\hat{\mathbf{f}}_{ML} &= (\mathbf{A}^T\mathbf{A})^{-1}\mathbf{A}^T\mathbf{r}_e \\ &= \mathbf{A}^{+}\mathbf{r}_e \\ &= \mathbf{V}\mathbf{\Sigma}^{+}\mathbf{U}^T\mathbf{r}_e\end{aligned} \tag{2}$$

where $\mathbf{A}^+$ is the pseudoinverse of $\mathbf{A}$, $\mathbf{U}$ and $\mathbf{V}$ are orthogonal matrices, and $\mathbf{\Sigma}^+$ is a diagonal matrix whose elements are given by the reciprocals of the singular values on the diagonal of the matrix $\mathbf{\Sigma}$ in the singular value decomposition $\mathbf{A} = \mathbf{U}\mathbf{\Sigma}\mathbf{V}^T$. If we require that the estimate $\hat{\mathbf{f}}_{ML}$ remain unbiased, then all components of the output space spanned by the columns of $\mathbf{V}$ must be retained. Recall that the ML estimate uses no *a priori* information about the image. These assumptions lead to an simple figure of merit which does not depend on the image details, but on the sampling geometry details defined by the matrix $\mathbf{A}$.

If the measurement vector is decomposed into its signal and zero-mean noise component, $\mathbf{r}_e = \bar{\mathbf{r}}_e + \mathbf{n}$, then we can consider the noisy portion of the linear inversion as

$$\mathbf{f}_N = \mathbf{V}\mathbf{\Sigma}^+\mathbf{U}^T\mathbf{n}. \tag{3}$$

We seek an appropriate statistic for the noise image vector $\mathbf{f}_N$. If the components of $\mathbf{n}$ are zero-mean, uncorrelated random variables of variance σ_I^2, then the average variance of the image pixels σ_O^2 can be written in the relationship

$$G = \frac{\sigma_O^2}{\sigma_I^2} = \frac{1}{n}\sum_{i=1}^{n}\frac{1}{\sigma_i^2} = \frac{1}{n}\sum_{i=1}^{n}\frac{1}{\lambda_i}. \tag{4}$$

We note that the square of the singular value σ_i^2 is the same as the eigenvalue λ_i of $\mathbf{A}^T\mathbf{A}$ for $i \leq n$. We will use this noise power gain as a figure of merit for the performance of the inversion. The number G depends solely on the distribution of the singular values of $\mathbf{A}$.

3. RANDOM SAMPLING SIMULATION DESCRIPTION

There exist a rich set of possibilities for random sampling strategies. The degrees of freedom include (at least) the transmit/receive configuration of the vehicles; the spatial distribution of the vehicles; and the distribution of sample ellipses used from a single transmit burst.

We choose a Monte Carlo simulation method in which the locations of many vehicles are drawn from a uniform distribution in a volume directly above a square image of interest, with heights varying from 1 to 2 image dimensions. The vehicles are paired into single transmit/receive units which generate sample ellipses of the general form (corrected from [1]):

$$x^2 + (1 - \frac{4d^2}{K^2})(y - \frac{d(h_1^2 - h_2^2)}{(K^2 - 4d^2)})^2 = \\ \frac{K^2}{4} - d^2 - \frac{h_1^2 + h_2^2}{2} + \frac{(h_1^2 - h_2^2)^2}{4(K^2 - 4d^2)} = r^2 \tag{5}$$

where the pair lies on some y axis at $x = \pm d$, h_i represent the heights of the vehicles over the plane, and K is the total distance traveled by a photon reflected from the transmitter to the receiver. We can re-parameterize the ellipses, replacing K with the number r, the semi-major axis of the ellipse. Starting with a small value, the ellipse parameter r is incremented by the pixel dimension δ_x until the ellipses become too large to interact with the image. This local y axis can be inclined at any angle with respect to the reference y axis of the image, depending on the bistatic pair's geometry. The simulation repeats this process until the desired number of line integral measurements, m, is reached or slightly exceeded.

4. RESULTS

We now summarize the performance results of the Monte Carlo simulations and compare these to the standard deterministic $\mathcal{R}_e f$ performance. All simulations in this work employ an image with $n = 50 \times 50$ pixels. First, we compare in detail the distribution of the first 2500 singular values of $\mathbf{A}$.

Figure 1 highlights a deterministic-looking distribution for the random sampling case, with a sharp cutoff at the low end, exhibiting no singular values below about $\sigma < 0.1$. By contrast, the deterministic version looks rather random; more importantly, it indicates that a large number of singular values exist near the origin.

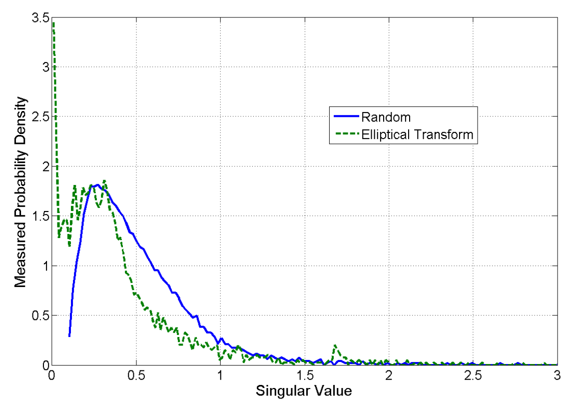

Fig. 1. The empirical singular value distributions of $\mathbf{A}$ for $\mathcal{R}_e f$ and for a random sampling trial, with $m \approx 12000$.

This small-σ difference shows up even more strikingly in the inversion performance shown in Figure 2. The results indicate that random sampling typically outperforms $\mathcal{R}_e f$ by 40 dB...a very substantial difference.

To verify the performance improvement due to random sampling methods, we implemented the full measurement and inversion process for a Shepp-Logan test image with measurements corrupted by a Gaussian noise of constant variance σ_I^2. Both $\mathbf{A}$ matrices had $m \approx 9000$. Figure 3 shows a side-by-side comparison the resulting images.

The random-sampling inversion is visually indistinguishable from a perfect image, while the $\mathcal{R}_e f$ inversion, while

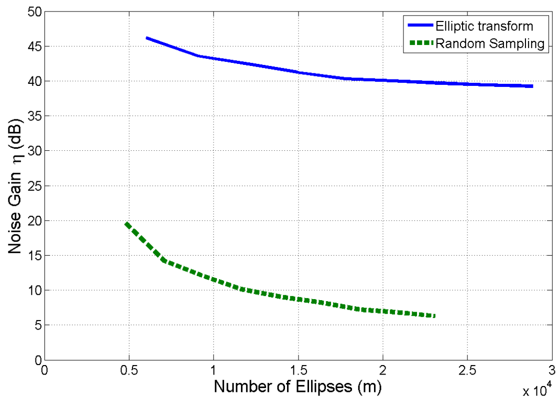

Fig. 2. Noise gain of deterministic and random sampling as a function of the measurement size m and constant $n = 50 \times 50$.

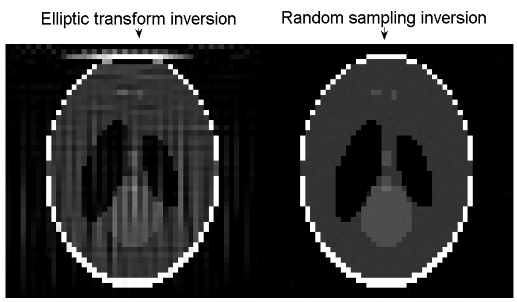

Fig. 3. Comparison of reconstructed images with the same measurement noise power, using $m \approx 9000$.

recognizable, is clearly inferior. The distortions in the $\mathcal{R}_e f$ image appear striped because the 2D eigenfunctions associated with the smallest singular values exhibit these types of shapes. Thus we see that random sampling produces stable inversions, and in fact can easily outperform the inversion of standard deterministic trajectories. These results are consistent with the findings of [6] for the inversion of the usual Radon transform.

5. APPLICATION OF RANDOM MATRIX THEORY

The non-zero elements of the sparse matrix $\mathbf{A}$ are the arc lengths of randomly placed ellipses cut by a rectangular grid. We now examine the consequences of treating the elements A_{ij} as random variables with marginal density function

$$p_x(x) = (1 - s)\delta(x) + sP_x(x) \tag{6}$$

where s is the sparsity of $\mathbf{A}$. For dense matrices ($s \approx 1$) with i.i.d. A_{ij} entries, large m and n with $\beta = n/m$, the eigen-

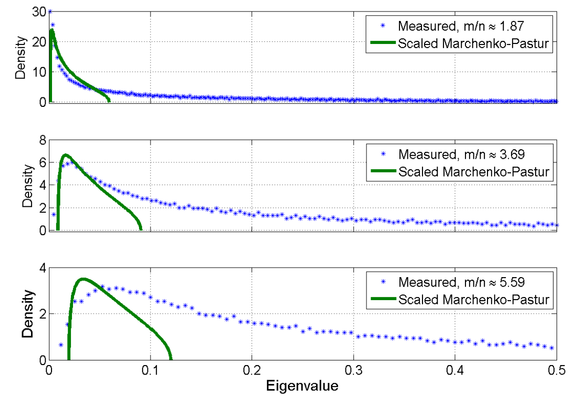

Fig. 4. Comparison of actual and Marchenko-Pastur eigenvalue densities of $\mathbf{A}^T\mathbf{A}$ for various $\gamma = m/n$.

values of $\mathbf{A}^T\mathbf{A}$ are distributed according to the Marchenko-Pastur (MP) asymptotic law [8]:

$$p_\lambda(\lambda) = \frac{1}{2\pi\beta m\sigma_A^2\lambda}\sqrt{(b-\lambda)(\lambda-a)} \tag{7}$$

where $\lambda > a = m\sigma_A^2(1-\sqrt{\beta})^2$, $\lambda < b = m\sigma_A^2(1+\sqrt{\beta})^2$, and σ_A^2 is the variance of A_{ij}. The general problem, with jointly distributed A_{ij} entries and $s \ll 1$, is open. Nagao and Tanaka [9] conclude that deviations from the MP law due to the sparsity in equation 6 are significant in the tail region of the spectrum. Figure 4 compares the actual and MP distributions for a particular instantiation of $\mathbf{A}$. The MP parameter σ_A^2 is calculated directly from the matrix. The MP density functions are scaled for easier comparison at small eigenvalues. We observe that the MP approximation describes the lower end of the distributions reasonably well in all cases. We also observe, in agreement with Nagao, that the deviations are most significant in the tail regions; in our case, the tail region deviations get more significant as m/n increases. The stochastic version of our figure of merit (equation 4) is the expectation of $1/\lambda$:

$$G_{MP} = E[\frac{1}{\lambda}] = \int_a^b \frac{1}{\lambda}p_\lambda(\lambda)d\lambda = \frac{1}{\sigma_A^2(m-n)} \tag{8}$$

which is the fundamental result of the present work. We note that because deviations occur at higher λ values , G_{MP} should be an asymptotic upper bound on the noise power gain of the inversion. Furthermore, because the tail deviations are attenuated by the factor $1/\lambda$, and have small $p_\lambda(\lambda)$, this upper bound may approximate the exact answer reasonably well. Figure 5 shows this upper bound G_{MP} using the nominal measured σ_A^2 of the matrices, an empirical measurement, and a best-fit G_{MP} using a modified value $\sigma_A'^2 = 2\sigma_A^2 = \eta\sigma_A^2$.

We see that our upper bound is exceeded at small matrix size. The matrix in this case may be too small to consistently

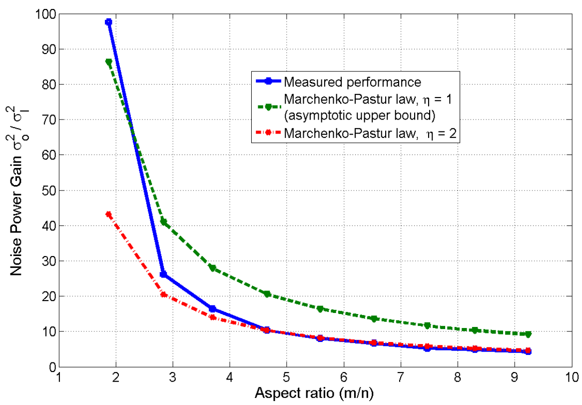

Fig. 5. Noise power gain versus $1/\beta = m/n$ showing an asymptotic upper bound, empirical measured data, and a best-fit model.

obey the MP law. At higher, more-useable values of m/n, we see that the price of neglecting the sparsity and the joint density of the random matrix $\mathbf{A}$ is a consistent factor of 2 in the input noise power.

Finally, we can recast equation 8 in terms of physical parameters of interest in the SAR system. It can be shown by simple counting arguments that the sparsity s of $\mathbf{A}$ is inversely proportional to $\sqrt{n}$. Therefore, the variance of A_{ij} is proportional to $\delta_x^2/\sqrt{n}$, where δ_x^2 is the area corresponding to a pixel in the reflectivity plane. But $\delta_x^2 = A/n$, where A is the area of the image. Therefore,

$$G_{MP} = \kappa \frac{n^{3/2}}{A(m-n)} \tag{9}$$

for some constant κ. Recall that the measurement noise has been modeled as i.i.d. Gaussian, which is approximately correct in the case where the SAR system noise is dominated by the electronic noise in the receiver amplifiers. Under this model, improvements in linear resolution on the same area require both the electronic noise bandwidth and the input noise variance σ_I^2 to increase proportionally with $\sqrt{n}$. Therefore the image noise variance can be expressed as

$$\sigma_O^2 = \kappa' \frac{n^2}{A(m-n)}. \tag{10}$$

Equations of this type are useful as scaling rules for system design. For example, consider a working SAR system in which $n = 10,000$ and which can process $m = 30,000$ measurements. According to equation 10, a new system needing twice the pixels over the same area will need to boost transmit power by 8 times (9 dB) to maintain the pixel quality of the old product. Alternatively, m could be increased to 100,000 without modification to the transmit power.

6. CONCLUSIONS

We have proposed random-location sampling methods for multistatic SAR in which a swarm of SAR vehicles at uncontrolled locations provides a set of measurements. We developed one (of many possible) random-sampling strategies and showed that this strategy can significantly outperform a deterministic sampling method which is prevalent in the literature. We applied the remarkable power of a central result in random matrix theory to produce a simple closed-form estimation of the pixel quality in a random SAR in terms of its system parameters.

Areas of interest for future extensions of this work include: improvement of the asymptotic performance bound by developing a better closed-form approximation to the eigenvalue distribution for this problem; comparison of alternative random-sampling strategies; and investigation of the effect of random sampling on other SAR inversion disturbances.

7. REFERENCES

[1] Jonathan D. Coker and Ahmed H. Tewfik, "Multistatic SAR image reconstruction based on an elliptical-geometry Radon transform," *International Waveform Diversity and Design Conference*, 2007.

[2] N.J. Redding, "SAR image formation via inversion of radon transforms," in *Image Processing, 2004. ICIP '04. 2004 International Conference on*, 2004, vol. 1, pp. 13–16.

[3] A. S. Milman, "The hyperbolic geometry of SAR imaging," 2006.

[4] Stephen J. Norton, "Reconstruction of a two-dimensional reflecting medium over a circular domain: Exact solution," *Journal of the Acoustical Society of America*, vol. 67, no. 4, pp. 1266, April 1980.

[5] Birsen Yazici Can E. Yarman and Margaret Cheney, "Bistatic synthetic aperture hitchhiker imaging," *ICASSP*, 2007.

[6] E. J. Candés and T. Tao, "Near-optimal signal recovery from random projections: Universal encoding strategies," Tech. Rep., Applied and Computational Mathematics, Calif. Inst. Technol., 2004.

[7] D. L. Donoho, "Compressed sensing," *IEEE Trans. on Information Theory*, vol. 52, no. 4, 2006.

[8] A. M. Tulino and S. Verdu, *Random Matrix Theory and Wireless Communications*, Now Publishers, 2004.

[9] Taro Nagao and Toshiyuki Tanaka, "Spectral density of sparse sample covariance matrices," *J. Phys. A: Math. Theor.*, vol. 40, 2007.